HHS Public Access

Author manuscript

Int J Radiat Oncol Biol Phys. Author manuscript; available in PMC 2024 March 15.

Published in final edited form as:

Int J Radiat Oncol Biol Phys. 2023 March 15; 115(4): 933–944. doi:10.1016/j.ijrobp.2022.10.012.

Manipulation of Redox Metabolism Using Pharmacologic Ascorbate Opens a Therapeutic Window for Radio-Sensitization by ATM Inhibitors in Colorectal Cancer

Cameron M. Callaghan, MD[*], **Ibrahim M. Abukhiran, MD**[†], **Amr Masaadeh, MD**[†], **Richard V. Van Rheeden, MS**[‡], **Amanda L. Kalen, MS**[*,§], **Samuel N. Rodman III, BS**[*,§], **Michael S. Petronek, MS**[*,§], **Kranti A. Mapuskar, PhD**[*,§], **Benjamin N. George, BS**[*], **Mitchell C. Coleman, PhD**[*,§], **Prabhat C. Goswami, PhD**[*,§], **Bryan G. Allen, MD, PhD**[*,§], **Douglas R. Spitz, PhD**[*,§], **Joseph M. Caster, MD, PhD**[*,§]

[*]Department of Radiation Oncology, University of Iowa Hospital and Clinics, Iowa City, Iowa

[†]Department of Pathology, University of Iowa Hospitals and Clinics and Carver College of Medicine, Iowa City, Iowa

[‡]Department of Pediatrics, The University of Iowa, Iowa City, Iowa

[§]Free Radical and Radiation Biology Program, Department of Radiation Oncology, Holden Comprehensive Cancer Center, University of Iowa, Iowa City, Iowa

Abstract

Purpose: Ataxia telangiectasia mutated kinase (ATM) inhibitors are potent radiosensitizers that regulate DNA damage responses and redox metabolism, but they have not been translated clinically because of the potential for excess normal tissue toxicity. Pharmacologic ascorbate ($P\text{-}AscH^-$; intravenous administration achieving mM plasma concentrations) selectively enhances H_2O_2-induced oxidative stress and radiosensitization in tumors while acting as an antioxidant and mitigating radiation damage in normal tissues including the bowel. We hypothesized that $P\text{-}AscH^-$ could enhance the therapeutic index of ATM inhibitor-based chemoradiation by simultaneously enhancing the intended effects of ATM inhibitors in tumors and mitigating off-target effects in adjacent normal tissues.

Methods and Materials: Clonogenic survival was assessed in human (human colon tumor [HCT]116, SW480, HT29) and murine (CT26, MC38) colorectal tumor lines and normal cells (human umbilical vein endothelial cell, FHs74) after radiation ± DNA repair inhibitors ± $P\text{-}AscH^-$. Tumor growth delay was assessed in mice with HCT116 or MC38 tumors after fractionated radiation (5 Gy × 3) ± the ATM inhibitor KU60019 ± $P\text{-}AscH^-$. Intestinal injury, oxidative damage, and transforming growth factor β immunoreactivity were quantified using immunohistochemistry after whole abdominal radiation (10 Gy) ± KU60019 ± $P\text{-}AscH^-$. Cell cycle distribution and ATM subcellular localization were assessed using flow cytometry and

Corresponding author: Joseph Caster, MD/PhD; josephcaster@uiowa.edu.

Disclosures: none.

Supplementary material associated with this article can be found in the online version at doi:10.1016/j.ijrobp.2022.10.012.

immunohistochemistry. The role of intracellular H_2O_2 fluxes was assessed using a stably expressed doxycycline-inducible catalase transgene.

Results: KU60019 with P-AscH$^-$ enhanced radiosensitization in colorectal cancer models in vitro and in vivo by H_2O_2-dependent oxidative damage to proteins and enhanced DNA damage, abrogation of the postradiation G2 cell cycle checkpoint, and inhibition of ATM nuclear localization. In contrast, concurrent P-AscH$^-$ markedly reduced intestinal toxicity and oxidative damage with KU60019.

Conclusions: We provide evidence that redox modulating drugs, such as P-AscH$^-$, may facilitate the clinical translation of ATM inhibitors by enhancing tumor radiosensitization while simultaneously protecting normal tissues.

Introduction

The generation of DNA double strand breaks (DSBs) is a key mechanism by which ionizing radiation (RT) induces cell death.[1] Ataxia telangiectasia mutated kinase (ATM) is a kinase that plays a key role in coordinating the DNA damage response.[2,3] In addition to its established roles in DNA repair, ATM is also involved in maintaining redox homeostasis and mounting antioxidant responses to oxidative stressors.[4-8] ATM-deficient cells demonstrate high levels of basal oxidative stress markers and reduced tolerance to oxidants, including hydrogen peroxide (H_2O_2).[9-11] ATM inhibitors are potent radiosensitizers in preclinical tumor models.[12-14] However, radiosensitization with ATM inhibitors is not specific to tumors, and their clinical translation has been limited because of potentially increased normal tissue toxicity.[15,16] ATM inhibitors significantly increase RT toxicity in rapidly dividing normal tissues, including skin and bowel in preclinical studies.[17,18] Novel strategies that selectively mitigate unintended radiosensitization in normal tissues without blunting the desired effects in tumors could facilitate the clinical application of ATM inhibitors as radiosensitizers for extracranial malignancies.

Ascorbate (AscH$^-$; vitamin C) acts as a reducing agent and donor antioxidant by undergoing consecutive oxidations under normal physiological conditions.[19] However, the kinetics of these reactions are context dependent; hence, AscH$^-$ can function as a pro- or antioxidant depending on cellular conditions. Pharmacologic ascorbate (P-AscH$^-$) specifically refers to high dose (75-100 g) intravenous administration, which produces much higher peak plasma concentrations (15-20 mM) than can be achieved with oral administration.[20-22] Numerous studies have shown that P-AscH$^-$ selectively functions as a prooxidant in tumors while exerting neutral or even protective effects in nonmalignant tissues.[21-25] The mechanism of selective toxicity in tumors is thought to be dependent on perturbations in tumor oxidative metabolism, which results in an excess of unpaired electrons and increased steady-state reactive oxygen species (ROS).[19,26,27] In the oxidizing environment in tumors, AscH$^-$ is oxidized to the ascorbate radical, which interacts with redox reactive metals and oxygen to form highly reactive intermediates (including superoxide), which ultimately result in the feedforward production of supraphysiological H_2O_2 fluxes.[19,23,24] In addition to these immediate effects, P-AscH$^-$ may also induce expression of nicotinamide adenine dinucleotide phosphate oxidase family members dual oxidase 1 and 2, which mediate sustained increases in oxygen consumption and H_2O_2 production.[28] H_2O_2 is a reactive

intermediate that induces oxidative stress after RT, but it is less reactive than oxygen radical species (superoxide and hydroxide radicals) and not a major source of lethal DNA double strand lesions after RT under physiological conditions. However, the supraphysiologic H_2O_2 fluxes generated by concurrent P-AscH$^-$ readily sensitize many tumors to DNA damaging oxidative stressors, including RT and chemotherapeutics.[21,23,24,29] Because ATM is a key redox sensor and post-RT DNA damage is influenced by intracellular redox status, we hypothesized that P-AscH$^-$ may be ideally suited to enhance tissue selectivity of ATM inhibitors as radiosensitizers. Here, we provide evidence that P-AscH$^-$ enhances radiosensitization with the ATM inhibitor KU60019 in human and syngeneic murine colorectal cancer (CRC) tumor models while simultaneously reducing excess radiation damage, oxidative stress markers, and expression of the profibrotic cytokine transforming growth factor (TGF)-β in the bowel. We further provide evidence that intracellular ROS fluxes enhanced by P-AscH$^-$ in tumors inhibit nuclear ATM localization and perturb cell cycle checkpoints after RT.

Methods and Materials

Cell culture

Human colon tumor (HCT)116, SW480, HT29, human umbilical vein endothelial cell (HUVEC), and FHs74-int cell lines were purchased from ATCC. B1 chinese hamster cells and the HCTllt doxycyline inducible cells were from Drs Douglas Spitz and Melissa Fath.[24] Murine CT26 and MC38 cells lines were from Drs Paloma Giangrande and Ralph Weichselbaum. HCT116, HCT Cat+, and SW480 were grown in Roswell Park Memorial Institute + 10% fetal bovine serum (FBS), and MC38 and B1 cells were grown in DMEM + 10% FBS. FHs74-int cells were grown in Hybri-Care Medium 46-X supplemented with 30 ng/mL human epidermal growth factor and 10% FBS. HUVEC cells were grown using the EGM Bullet kit (Lonza Walkersville).

P-AscH$^-$ treatments were performed in media + 10% FBS equilibrated in 5% CO_2, 4% O_2, 37°C for at least 1 hour. P-AscH$^-$ stock solutions (0.95-1.05 M [pH 7]) were made under argon and stored at 4°C. In vitro RT was delivered using a Cesium irradiator with dose rate of 0.596 Gy/min. DNA repair inhibitors (DRIs) were purchased from SelleckChem, dissolved in dimethylsulfoxide at a stock concentration of 1 mM, and stored at −20°F. For in vitro drug treatments, DRIs were diluted to final concentrations in growth media for 24 hours; 1 μM for KU-60019 and VE-821 and 5 μM for Veliparib (ABT-888). Control cells were treated with an equal volume of dimethylsulfoxide vehicle. P-AscH$^-$ pretreatment started 2 hours after the start of DRI treatment and RT was delivered 1 hour after P-AscH$^-$ administration.

Clonogenic survival

Cells were plated and maintained at 37°C and 4% O_2 for 24 to 48 hours before treatment. Cells were washed, trypsinized, and plated immediately after RT. Each biological replicate was plated in triplicate and represents the average number of colonies from the triplicates. All conditions were repeated for a minimum of 3 independent biological replicates. Cloning dishes were incubated for 7 to 14 days to allow for colony formation. FHs74-Int cells were

plated on top of Chinese hamster fibroblast (B1 designation) feeder cells (1×10^5 per well) that had been irradiated to 30 Gy. Colonies were fixed in 70% ethanol and stained with Coomassie blue. Colonies containing ≥30 cells were counted.

Neutral COMET assay

Samples were resuspended in phosphate buffered saline (PBS), mixed 1:10 in agarose, and plated onto slides. Slides were placed in prechilled lysis solution and incubated overnight at 4°C. Electrophoresis was performed in neutral buffer solution at 1 V/cm for 45 minutes at 4°C. Slides were incubated sequentially in DNA precipitation solution, 70% ethanol, and finally 100 uL of SYBR gold (Thermo Fisher) 1:30,000 in TE buffer per slide for 30 minutes in the dark at room temperature. Slides were then washed and imaged using an Olympus CKX41 (Evident Corp, Olympus Scientific Solutions Americas DBA, Waltham, MA) Inverted Phase Contrast Microscope and a Prior Lumen L200US (Prior Scientific, Rockland, MA) light source. COMETs were then quantified using OpenComet (v1.3.1) and ImageJ (version 1.53) software.

Cell cycle distribution and flow cytometry

Asynchronous exponentially growing cells were harvested 5 hours posttreatment and analyzed for cell cycle phase distributions using flow cytometry measurements of DNA content as previously described.[30] Ethanol-fixed cells were resuspended in PBS and treated with RNase A (1 mg^{-mL}; Thermo Fisher) and propidium iodide (PI) (35 ng^{-mL}). Cell cycle phase distributions for the extended timepoints were analyzed by bromodeoxyuridine (BrdU) pulse labeling followed by flow cytometry analysis of DNA content. Cells were incubated with BrdU (1 mM) for 30 min before ethanol fixation. Cells were resuspended in 0.2 mg^{-mL} pepsin (Sigma) in 2 N HCL, neutralized (0.1 M Borax, pH 8.5), and incubated with anti-BrdU primary antibody (BD Biosciences) and fluorescein isothiocyanate-conjugated secondary antibody (BD Biosciences) followed by incubation with RNAase A and PI. At least 10,000 events were recorded for each sample. LSR II flow cytometer (Becton Dickinson), ModFit (version 4.1.7), and FlowJo (version 10.7.2) software were used to identify and analyze cell cycle phase distributions.

Immunofluorescence

Cells were plated on glass slides with wells and incubated at 37°C and 4% O_2 for 24 to 48 hours before treatment. Immediately after treatment, cells were washed in PBS and fixed in 4% paraformaldehyde for 10 min, permeabilized in 0.1% Triton X-100 for 10 minutes, blocked with 3% bovine serum albumin in PBS for 1 hour at room temperature, and incubated with primary antibody (pATM Ser1981 [Invitrogen]; ATM [Cell Signaling] 1:500 in 3% bovine serum albumin) overnight at 4°C. Secondary antibodies were applied for 1 hour at room temperature (1:500 in PBS, Alexa Fluor 488 goat antimouse [Thermo Fischer]) and stained with rhodamine phalloidin (Thermo Fischer) and 4'−6-diamidino-2-phenylindole (DAPI) slowfade mountant (Thermo Fischer) for 10 minutes. Images were captured using Olympus FV1000 Laser Scanning Confocal based on an Olympus BX61WI microscope at 40X magnification. Images were quantified using ImageJ software (version 1.53). At least 100 cells per condition in each of 3 biological replicates were used for quantification by blinded reviewers.

Subcellular localization of total ATM was assessed using Image J Software (version 1.53). Nuclear and cytoplasmic fractions were quantified as the proportion of ATM that colocalized with DAPI and cytokeratin, respectively. High intensity pATM foci were also quantified using image J Software. For each cell line and biologic replicate, the contrast on the pATM images in the control cells was adjusted to exclude background signal, and this setting was applied to all additional samples in that biologic replicate. Nuclear (DAPI-colocalized) foci were then automatically counted and divided by the total number of cells per image. All images were analyzed by a reviewer who was blinded to the treatment conditions.

Murine models

All animal studies and procedures were approved by the institutional animal care and use committee at the University of Iowa. Eight-week-old male and female C57BL/6J and Athymic-nude *FOXn1*$^{nu/nu}$ mice were purchased from Jackson Laboratories and Envigo, respectively. KU60019 was administered at 0.5 mg/kg via tail vein injection and P-AscH^{-} at 4 g/kg via intraperitoneal injection dosed 3 hours before radiation (when drug and RT were administered on the same days). Controls were given the same volume of 0.9% normal saline. Doxycycline was administered via the water supply at 2 mg/mL in 1% sucrose. RT was delivered using a Small Animal Radiation Research Platform at dose rate of 2.5 Gy/min using a 220 kVp x-ray beam with a quality of 0.66 mm Cu. Calibration of this beam was performed in accordance with the AAPM TG-61 protocol for x-rays. Mice were anesthetized for RT using ketamine/xylazine (100/10 mg/kg) and positioned on their left sides in the restraints so that tumors were enface with respect to the radiation beam. Tumors were left exposed for radiation and mice were shielded using 2 layers of 3-mm lead shielding affixed to the restraints. Adequate tumor exposure and animal shielding was verified by visual inspection on the treatment platform before each treatment.

C57bl/6j mice were inoculated with 1.0×10^6 MC38 cells in PBS and Matrigel (1:1) and subcutaneously injected with 100 uL total volume into unilateral (right) flanks. Xenograft models used Athymic-nude *FOXn1*^{nu} mice inoculated with 5.5×10^6 HCT116 Cat+ cells 1:1 with Matrigel of 100 μL final volume. Mice were randomly assigned to experimental groups (5-15 mice per group) when tumors reached approximately 5 mm in greatest dimension. Tumor volumes were assessed every 2 to 3 days after completion of treatment by measuring the tumor length and width and using the formula $Tv = 0.5 \times L \times W^2$. Animals were euthanized when tumors reached 20 mm in largest diameter.

Immunohistochemistry

For acute bowel toxicity studies, mice were euthanized3.5 days after RT. Jejunal and rectal tissue samples were fixed in formalin and sectioned for hematoxylin and eosin stain (H&E) and immunohistochemistry staining for 4-hydroxynoneal (4HNE) (Abeam), 3-nitrotyrosine (3NT) (Millipore), and TGF-β_1 (Santa Cruz Biotechnology). Samples were scored by a blinded pathologist for H&E acute toxicity, jejunal crypt density (crypts/mm entire circumference), 4HNE, 3NT, and TGF-β_1 for jejunal samples and rectal injury score for rectal samples.

Catalase activity assay

Catalase activity was determined on both cell samples and whole mouse tumor homogenized in 50 mM potassium phosphate buffer (pH 7.8, with 1.34 mM diethylenetriaminepentaacetic acid). Activity (expressed as m*k* units/mg of protein) was determined by measuring the disappearance of 10 mM hydrogen peroxide (240 nm) as previously described.[31] In vitro samples were prepared after 48 hours incubation ± 4 uL of 1 mg/mL of doxycycline in 4 mL media. In vivo samples of Cat+ tumors were inoculated as previously discussed, and mice were administered water with 1% sucrose ± 2 mg/mL doxycycline for 48 hours.

Statistical analysis

Beta regression models were used for cell cycle experiments and clonogenic survival assays with Bonferroni testing for multiple comparisons. Wilcoxon rank sum tests were used for H&E acute toxicity score, rectal injury scores, and immunohistochemistry staining scores. Linear regression was used to assess clonogenic survival and jejunal crypt density. Linear and nonlinear mixed effects regression models were used to estimate and compare tumor growth and weight changes. The Kaplan-Meier method was used to estimate survival curves, and treatment group comparisons were made using the log rank test using SAS v9.4 (SASqPCR). Experiments with linear scale continuous variables, including tail moment for COMET assays, pATM and total ATM integrated densities, and pATM high intensity foci, were assessed using analysis of variance and, when indicated by significant main effects, post hoc group comparisons were made using Tukey test for multiple comparisons (Prism Software). All statistical analyses were 2-sided and assessed at the 5% significance level.

Results

P-AscH$^-$ enhances radiosensitization and DNA damage with ATM inhibition in CRC tumor models

We hypothesized that P-AscH$^-$ would enhance the combined effects of RT and ATM inhibitors. Because prior studies have demonstrated that P-AscH$^-$ induces DNA damage (with or without radiation) in tumors,[21,27] we further predicted that P-AscH$^-$ would also enhance the sensitizing effects of other classes of DRIs that are also in clinical development, including inhibitors ATR and PARP. CT26 and MC38 cells were treated with RT (0-8 Gy) and varying doses of VE821 (ATR, 0.5-5 μM), KU60019 (ATM, 0.5-5 μM), and veliparib (PARP, 1-25 μM), and we found that doses ≥1 μM VE821 and KU60019 and 5 μM veliparib enhanced radiosensitization in both lines (Fig. E1A). To test for enhanced radiosensitization with P-AscH$^-$ and DRIs, human (HCT116, HT29, SW480) and murine (CT26, MC38) CRC cells were treated with radiation (5 Gy) ± DRIs ± P-AscH$^-$ (5 pmol/cell). All 3 of the tested DRIs enhanced radiosensitivity in all tumor lines tested compared with radiation alone (Figs. 1A and E1B). P-AscH$^-$ further enhanced cell killing with RT and DRIs in most of the lines tested, as analysis of variance indicated a main effect of ascorbate in all lines except for HT29 (Figs. 1A and E1B). P-AscH$^-$ enhances radiosensitivity by inducing H_2O_2 fluxes in tumors,[23,24] and we predicted that the interactions between P-AscH$^-$ and DRIs was also H_2O_2 dependent. We tested this hypothesis using HCT116 tumors stably expressing a doxycycline-inducible catalase transgene.[24] As predicted, catalase induction completely abrogated the added toxicity of P-AscH$^-$ with RT ± DRIs but had no significant effect

on clonogenic survival in the absence of ascorbate (Fig. 1B). Additional studies focused on ATM inhibition because ATM is a key sensor of both DSBs and ROS, and KU60019 induced more radiosensitization than other DRIs in most cell lines tested.

Because ATM inhibitors and P-AscH$^-$ both enhance DNA damage after RT, we hypothesized that the combination would induce more DNA damage than either drug alone. DNA damage was quantified using neutral COMET assays 0 and 24 hours after treatment with RT (5 Gy) ± KU60019 ± P-AscH$^-$ in HCT116 cells (Fig. 1C,D). As expected, P-AscH$^-$ directly induced DNA damage as indicated by a significant increase in tail moment with P-AscH$^-$ compared with control. KU60019 markedly increased post-RT DNA damage and the addition of P-AscH$^-$ to KU60019 and RT significantly increased tail moment compared with all other treatments, suggesting that combination therapy with P-AscH$^-$ and KU60019 induces more DNA damage immediately after RT than either agent alone (Fig. 1D).

We then assessed the in vivo radiosensitizing potential of P-AscH$^-$ and KU60019 using a fractionated course of RT (5 Gy × 3) in mice bearing MC38 or HCT116 Cat+ tumors (Fig. 2). In MC38 tumors, the combination of RT+ P-AscH$^-$ + KU60019 induced longer tumor growth delay and survival than all other combinations (Fig. 2A). In HCT116 tumors, KU60019 and KU60019 + P-AscH$^-$ induced longer tumor growth delay than RT alone, but only combination therapy with RT + P-AscH$^-$ + KU60019 significantly improved survival compared with RT alone (Fig. 2B). Induction of catalase in HCT Cat+ tumors with oral doxycycline attenuated the effects of combination therapy with P-AscFP and KU60019 on both tumor growth delay and survival (Fig. 2C).

P-AscH$^-$ reduces oxidative damage and intestinal injury after RT and ATM inhibition

A key aspect of P-AscH$^-$ is that sensitization to RT should be specific to tumors and not normal tissues.[21,23] Clonogenic survival was assessed after RT ± KU60019 ± P-AscH$^-$ in cultured FHS-74 intestinal epithelial cells and HUVECs. RT dose-dependently decreased survival in both cell lines, and KU60019 significantly enhanced radiosensitization in FHS-74 enterocytes (Fig. 3A). P-AscH$^-$ did not induce radiosensitization in either nonmalignant cell line. Instead, there was a trend toward improved survival with P-AscH$^-$. Similarly, in contrast to tumor cells, P-AscH$^-$ did not enhance DNA damage in FHS 74-int cells as a monotherapy or in combination with RT (Fig. 3B). Because the bowel is comprised of numerous cell populations that respond differently to RT and mediate whole-organ responses to RT, we next assessed protective effects of P-AscH$^-$ in the bowel using tumor-free mice treated with a single fraction of whole abdominal RT (WART) (10 Gy) ± KU60019 (0.5 mg/kg intravenous × 5 days) ± P-AscH (4 g/kg intraperitoneal × 5 days) (Figs. 4 and E3). Gastrointestinal toxicity was functionally assessed posttreatment measuring weight loss (Fig. E3A). Mice treated with WART and KU60019 had significantly more acute weight loss than all other treatment groups, whereas mice treated with concurrent P-AscH$^-$ had no weight loss compared with control mice. We quantified markers of acute RT toxicity and oxidative damage in jejunal and rectal tissues harvested 3 days after treatment (Fig. 4). RT + KU60019 significantly increased H&E score in the rectum and jejunum and significantly decreased jejunal crypt density compared with RT alone. P-AscH$^-$ completely abrogated the excess architectural changes seen with RT + KU60019.

Intestinal 4HNE was increased with RT ± KU60019 but not with P-AscH$^-$ coadministration. A similar trend was observed with 3NT though this did not reach significance ($P = .063$). Redox-mediated activation of the fibrogenic cytokine TGF-β has been strongly implicated in post-RT fibrosis.[32,33] We next determined the effects of P-AscH$^-$ on intestinal TGF-β immunoreactivity after RT ± KU60019 (Fig. 4B). Intestinal TGF-β was significantly increased after RT ± KU60019, and concurrent P-AscH$^-$ reduced TGF-β immunoreactivity to control levels for both conditions.

P-AscH$^-$ perturbs G_2 checkpoint and early G_2 accumulation in CRC with RT ± KU60019

Next, we determined whether the enhanced toxicity observed in the combination treatments could result from changes in cell cycle checkpoint activation. Experimental designs used for the clonogenic assays were used to analyze cell cycle phase distributions 5 hours posttreatment (Figs. 5A,B and E4A). Although there were minimal changes in other cell cycle phases, P-AscH$^-$ significantly decreased the proportion of cells in G_2/M-phase after RT ± KU60019 in all lines except for HT29 (the only line tested that is not sensitized by P-AscH$^-$) (Fig. 5B). As with radiosensitization and DNA damage, cell cycle phase rearrangements were abrogated by catalase overexpression (Fig. 5B). These results suggest that radiosensitization by P-AscH$^-$ may at least in part be due to H_2O_2-mediated suppression or override of the G_2 checkpoint pathway.

Previous studies reported 2 distinct radiation-induced G_2 checkpoints: an early checkpoint that is ATM dependent and a late G_2 accumulation that is ATM independent.[34-36] To determine whether RT-induced G_2 accumulation is perturbed by the combination treatments, experiments were expanded to include additional posttreatment times. Cell cycle phase distributions were analyzed by flow cytometry analysis of BrdU pulse-labeled cells (Fig. 5C,D). As anticipated, RT increased accumulation of cells in G_2 phase beginning 5 hours posttreatment that peaked 24 hours posttreatment (Fig. 5C,D; remaining cell cycle phases are shown in Fig. E4B). P-AscH$^-$ further enhanced RT-induced G_2 accumulation at 24 hours posttreatment. Interestingly, inhibition of ATM suppressed (or overrode) this accumulation, probably by forcing cells into unscheduled entry into the M phase, resulting in enhanced toxicity. The effect of combination therapy on induced G_2-accumulation was suppressed in cells overexpressing catalase (Fig. 5D). Overall, these results suggest that P-AscH$^-$ initially inhibits RT-induced G_2 cell cycle checkpoint activation (5-12 hours) and facilitates RT-induced G_2-accumulation at later timepoints (24-48 hours). Furthermore, inhibition of ATM significantly suppressed (or overrode) P-AscH$^-$-induced enhancement of RT G_2 accumulation. H_2O_2 appears to regulate both pathways, the G_2 checkpoint and G_2 accumulation of CRC cells.

P-AscH$^-$-induced H_2O_2 fluxes reduce nuclear ATM localization after RT

Previous studies have found that exogenous treatment with H_2O_2 can fix ATM in an active homodimer that is preferentially localized in the cytoplasm.[4] Because P-AscH$^-$ induces H_2O_2 fluxes in tumor cells, we predicted that it would also affect post-RT ATM subcellular localization. We first assessed nuclear versus cytoplasmic localization of total ATM after RT and P-AscH$^-$ (Fig. 6A). As expected, RT (5 Gy) induced prominent nuclear localization of ATM. However, pretreatment with P-AscH$^-$ significantly reduced the fraction of ATM

localized to the nucleus and increased the cytoplasmic fraction after RT (but not with catalase overexpression). This suggests that P-AscH$^-$ decreases nuclear ATM localization after RT even though it also increases DNA damage. We next determined whether changes in subcellular ATM localization with P-AscH$^-$ post-RT also affected localization of pATM to sites of DNA damage by quantifying high-intensity nuclear foci 0, 2, and 24 hours after treatment (Figs. 6B and E5). RT significantly increased the number of foci per nucleus in all tested cell lines within 2 hours. This effect was reduced with concurrent P-AscH$^-$, except when catalase expression was induced by doxycycline. We also quantified total nuclear pATM intensity (integrated density) and observed similar results (Fig. E5).

Discussion

ATM inhibitors are among the most potent radiosensitizers identified, but they have not been clinically translated for this purpose in part due to concerns of the potential for excessive normal tissue toxicity. Several trials combining novel ATM inhibitors with palliative RT are open to accrual (NCT05002140, NCT03423628), but to our knowledge, no trials using definitive or preoperative RT have been initiated. Here, we provide preclinical evidence that tissue selective redox modulating drugs like P-AscH$^-$ may provide a promising opportunity to facilitate the clinical translation of ATM inhibitors for extracranial diseases by simultaneously enhancing their antitumor efficacy and mitigating unintended toxicity in adjacent normal tissues including the bowel and rectum. This line of research may be particularly relevant for diseases like locally advanced rectal cancer, for which there is a growing interest in nonoperative management for patients with complete responses to neoadjuvant therapy to reduce long-term complications.[37,38] By simultaneously enhancing tumor responses and decreasing post-RT bowel injury, combination therapy with P-AscH$^-$ and ATM inhibitors may represent a novel approach to addressing the antagonistic objectives of increasing desired responses in tumors while minimizing normal tissue effects. Our in vitro studies further suggest that P-AscH$^-$ may effectively enhance the radiosensitizing effects of other classes of DRIs, including inhibitors of ATR and PARP. Even though our current study focused on colorectal cancer, this novel approach may be directly applicable to other common abdominopelvic malignancies.

Our study provides evidence that redox modulating drugs like P-AscH$^-$ may be ideally suited to improve the tissue selectivity of ATM inhibitors that also modulate redox homeostasis.[9-11] DNA DSBs and ROS can independently activate ATM by distinct mechanisms. DSBs stimulate auto-phosphorylation of ser1981 and activation of monomeric ATM in the nucleus.[3] ROS can directly activate ATM via oxidation of the cys2991 residue located in the c-terminal domain.[4] In contrast to DSBs, oxidation of ATM by ROS fixes it in an active homodimer, which is translocated into the cytoplasm. RT can activate ATM via both pathways as it generates DSBs and intracellular ROS. Numerous studies have shown that ATM inhibition increases DNA DSBs post-RT. Here, we show that acute inhibition of ATM with KU60019 also significantly increases RT-mediated intestinal oxidative damage, as evidenced by increased immunoreactivity with 4HNE and 3NT. P-AscH$^-$ reverses this effect in the normal bowel, presumably by functioning as a donor antioxidant and reducing the effects of resultant ROS in the bowel. In contrast, in tumors we found that P-AscH$^-$ decreases post-RT nuclear ATM localization in a peroxide-dependent manner even though it

also increased DNA damage. This raises the possibility that in addition to directly inducing oxidative damage to DNA bases, P-AscH$^-$ may also enhance the efficacy of ATM inhibitors in tumors by inducing ATM homodimer formation and cytoplasmic localization and thereby reducing the ability of ATM to efficiently coordinate DSB repair post-RT.

We also provide preclinical evidence that P-AscH$^-$ may inhibit RT-mediated redox activation of profibrotic signaling pathways in the bowel. Numerous lines of evidence suggest that redox-mediated activation of the fibrogenic cytokine TGF-β is a key event in the induction and maintenance of post-RT fibrosis.[33,39-41] Importantly, fibrogenic signaling by TGF-β is at least partially self-propagating, and acute activation contributes to maintained fibrotic processes.[42,43] One of the key targets of canonical TGF-β signaling is the SMAD family of transcription factors, which mediate transcription of inflammatory and fibrogenic cytokines including platelet-derived growth factor, connective tissue grwoth factor, and TGF-β. TGF-β-SMAD2/3 signaling can also increase basal ROS production, which can further promote feedforward signaling between ROS and fibrotic pathways.[44,45] Our observation that P-AscH$^-$ inhibits increased intestinal TGF-β post-RT suggests that it may potently inhibit redox-mediated activation of profibrotic signaling. Additional mechanistic studies are needed to directly test our hypothesis, but our observations here provide preliminary evidence that P-AscH$^-$ may effectively inhibit redox-mediated activation of key fibrogenic signaling, which could potentially translate into a reduced risk of chronic bowel fibrosis post-RT.

A major strength of our study is that we propose a novel therapeutic approach that could be readily assessed in prospective clinical trials. Compared with other cancer therapies, P-AscH$^-$ is relatively inexpensive and readily available, and the feasibility of its administration with concurrent chemoradiation has been demonstrated in prospective clinical trials.[21,22] Additionally, unlike most other classes of radiosensitizers/radioprotectors, the tissue selectivity of P-AscH$^-$ affords an opportunity to simultaneously enhance the intended effects of radiation and ATM inhibitors in tumors while minimizing treatment toxicity. Other classes of tissue-selective redox- modulating drugs, including superoxide dismutase mimetics, have shown similar potential in preclinical and clinical studies.[46,47] Given their mechanistic similarities, it is possible these drugs could also enhance the tissue specificity of ATM inhibitors. Despite these strengths, our study has several important limitations. Consistent with previous studies,[21,25] we found that P-AscH$^-$ increased DNA damage with or without RT and DRIs. However, COMET assays provide little information regarding the specific types of DNA lesions induced by different treatments or combinations. P-AscH$^-$ alone significantly increased tail moment compared with control but had minimal effect on cell survival as a monotherapy, suggesting many of the DNA lesions stimulated by H_2O_2 fluxes are not inherently lethal. We also provide evidence of in vivo intestinal radioprotection with P-AscH$^-$ using high-dose single fraction (10 Gy) WART. Although this fractionation scheme closely approximates doses used in stereotactic body RT, most patients with abdominal and pelvic malignancies are treated with more fractionated radiation (1.8-2.0 Gy per day) over 5 to 6 weeks. Additionally, our pathologic endpoints focused on acute toxicity endpoints. Although acute and chronic enteropathy share some mechanistic overlap, acute enteropathy is generally reversable, and only a subset of patients with acute symptoms develop chronic enteropathy.[32] We hypothesize that a reduction in acute intestinal pathology

with P-AscH$^-$ will translate into reduced risk of irreversible chronic complications, but this was not directly tested in our current studies. Despite these limitations, our present results provide evidence of a novel, mechanism-based approach to improve the therapeutic index of ATM inhibitor-based chemoRT, which could be readily tested in patients.

In conclusion, we provide evidence that P-AscH$^-$ can enhance the antitumor efficacy of ATM inhibition and RT in several colorectal tumor models while simultaneously mitigating unintended toxicity in the bowel by selectively enhancing oxidative stress in tumors and reducing it refers to oxidative stress in the bowel. Collectively, our preclinical studies suggest tissue-selective redox modulating drugs like P-AscH$^-$ may be ideally suited to improve the efficacy and tolerability of ATM inhibitors as radiosensitizers. Successful demonstration of effective radioprotection with P-AscH$^-$ and ATM inhibitors in patients could offer a much-needed pathway for the broader adoption of these potent radiosensitizers for clinical use.

Supplementary Material

Refer to Web version on PubMed Central for supplementary material.

Acknowledgments

The authors would like to acknowledge Dr Michael McCormick for performance of catalase activity assays and Gareth Smith for the illustrations and figure formatting. The data presented herein also were obtained at the Flow Cytometry Facility, and statistical analyses were supported by the Biostatistical Core; both are Carver College of Medicine/Holden comprehensive Cancer Center core research facilities at the University of Iowa. These facilities are funded through user fees and the generous financial support of the Carver College of Medicine, Holden Comprehensive Cancer Center, and Iowa City Veterans Administration Medical Center.

Sources of support:

This work was supported by P01CA217797, P30CA086862, P01CA244091, T32CA078586, RSNA Research Resident Grant #RR1914, RSNA Research Scholar Grant #RSC2009, Gateway for Cancer Research award G-17-1500T32-GM007337, and the UIHC-CCOM Iowa Aging Initiative.

Data sharing statement:

All data generated and analyzed during this study are included in this published article (and its supplementary information files).

References

1. Rodemann HP. Molecular radiation biology: Perspectives for radiation oncology. Radiother Oncol 2009;92:293–298. [PubMed: 19726094]
2. Matsuoka S, Ballif BA, Smogorzewska A, et al. ATM and ATR substrate analysis reveals extensive protein networks responsive to DNA damage. Science 2007;316:1160–1166. [PubMed: 17525332]
3. Lavin MF, Kozlov S. ATM activation and DNA damage response. Cell Cycle 2007;6:931–942. [PubMed: 17457059]
4. Guo Z, Kozlov S, Lavin MF, Person MD, Paull TT. ATM activation by oxidative stress. Science 2010;330:517–521. [PubMed: 20966255]
5. Shimura T, Kobayashi J, Komatsu K, Kunugita N. Severe mitochondrial damage associated with low-dose radiation sensitivity in ATM- and NBS1-deficient cells. Cell Cycle 2016;15:1099–1107. [PubMed: 26940879]

6. Guo QQ, Wang SS, Zhang SS, et al. ATM-CHK2-Beclin 1 axis promotes autophagy to maintain ROS homeostasis under oxidative stress. EMBO J 2020;39e103111. [PubMed: 32187724]
7. Ditch S, Paull TT. The ATM protein kinase and cellular redox signaling: Beyond the DNA damage response. Trends Biochem Sci 2012;37:15–22. [PubMed: 22079189]
8. Agathanggelou A, Weston VJ, Perry T, et al. Targeting the ataxia telangiectasia mutated-null phenotype in chronic lymphocytic leukemia with pro-oxidants. Haematologica 2015;100:1076–1085. [PubMed: 25840602]
9. Reichenbach J, Schubert R, Schindler D, Muller K, Bohles H, Zielen S. Elevated oxidative stress in patients with ataxia telangiectasia. Antioxid Redox Signal 2002;4:465–469. [PubMed: 12215213]
10. Takao N, Li Y, Yamamoto K. Protective roles for ATM in cellular response to oxidative stress. FEBS Lett 2000;472:133–136. [PubMed: 10781820]
11. Kamsler A, Daily D, Hochman A, et al. Increased oxidative stress in ataxia telangiectasia evidenced by alterations in redox state of brains from ATM-deficient mice. Cancer Res 2001;61:1849–1854. [PubMed: 11280737]
12. Ivanov VN, Wu J, Wang TJC, Hei TK. Inhibition of ATM kinase upregulates levels of cell death induced by cannabidiol and gamma-irradiation in human glioblastoma cells. Oncotarget 2019;10:825–846. [PubMed: 30783513]
13. Biddlestone-Thorpe L, Sajjad M, Rosenberg E, et al. ATM kinase inhibition preferentially sensitizes p53-mutant glioma to ionizing radiation. Clin Cancer Res 2013;19:3189–3200. [PubMed: 23620409]
14. Zhang T, Shen Y, Chen Y, Hsieh JT, Kong Z. The ATM inhibitor KU55933 sensitizes radioresistant bladder cancer cells with DAB2IP gene defect. Int J Radiat Biol 2015;91:368–378. [PubMed: 25585815]
15. Choi S, Gamper AM, White JS, Bakkenist CJ. Inhibition of ATM kinase activity does not phenocopy ATM protein disruption: Implications for the clinical utility of ATM kinase inhibitors. Cell Cycle 2010;9:4052–4057. [PubMed: 20953138]
16. Weber AM, Ryan AJ. ATM and ATR as therapeutic targets in cancer. Pharmacol Ther 2015;149:124–138. [PubMed: 25512053]
17. Caster JM, Yu SK, Patel AN, et al. Effect of particle size on the biodistribution, toxicity, and efficacy of drug-loaded polymeric nanoparticles in chemoradiotherapy. Nanomedicine 2017;13:1673–1683. [PubMed: 28300658]
18. Tian X, Lara H, Wagner KT, et al. Improving DNA double-strand repair inhibitor KU55933 therapeutic index in cancer radiotherapy using nanoparticle drug delivery. Nanoscale 2015;7:20211–20219. [PubMed: 26575637]
19. Petronek MS, Stolwijk JM, Murray SD, et al. Utilization of redox modulating small molecules that selectively act as pro-oxidants in cancer cells to open a therapeutic window for improving cancer therapy. Redox Biol 2021;42 101864. [PubMed: 33485837]
20. Mehdi Z, Petronek MS, Stolwijk JM, et al. Utilization of pharmacological ascorbate to enhance hydrogen peroxide-mediated radiosensitivity in cancer therapy. Int J Mol Sci 2021;22:10880. [PubMed: 34639220]
21. Alexander MS, Wilkes JG, Schroeder SR, et al. Pharmacologic ascorbate reduces radiation-induced normal tissue toxicity and enhances tumor radiosensitization in pancreatic cancer. Cancer Res 2018;78:6838–6851. [PubMed: 30254147]
22. Allen BG, Bodeker KL, Smith MC, et al. First-in-human phase I clinical trial of pharmacologic ascorbate combined with radiation and temozolomide for newly diagnosed glioblastoma. Clin Cancer Res 2019;25:6590–6597. [PubMed: 31427282]
23. Schoenfeld JD, Sibenaller ZA, Mapuskar KA, et al. O2(−) and H2O2-mediated disruption of Fe metabolism causes the differential susceptibility of NSCLC and GBM cancer cells to pharmacological ascorbate. Cancer Cell 2017;32:268.
24. Brandt KE, Falls KC, Schoenfeld JD, et al. Augmentation of intracellular iron using iron sucrose enhances the toxicity of pharmacological ascorbate in colon cancer cells. Redox Biol 2018;14:82–87. [PubMed: 28886484]
25. Du J, Cieslak JA 3rd, Welsh JL, et al. Pharmacological ascorbate radio-sensitizes pancreatic cancer. Cancer Res 2015;75:3314–3326. [PubMed: 26081808]

26. Aykin-Burns N, Ahmad IM, Zhu Y, Oberley LW, Spitz DR. Increased levels of superoxide and H2O2 mediate the differential susceptibility of cancer cells versus normal cells to glucose deprivation. Biochem J 2009;418:29–37. [PubMed: 18937644]
27. Schoenfeld JD, Sibenaller ZA, Mapuskar KA, et al. O2(−) and H2O2-mediated disruption of Fe metabolism causes the differential susceptibility of NSCLC and GBM cancer cells to pharmacological ascorbate. Cancer Cell 2017;31 487–500.e8. [PubMed: 28366679]
28. Gibson AR, O'Leary BR, Du J, et al. Dual oxidase-induced sustained generation of hydrogen peroxide contributes to pharmacologic ascorbate-induced cytotoxicity. Cancer Res 2020;80:1401–1413. [PubMed: 32041838]
29. O'Leary BR, Houwen FK, Johnson CL, et al. Pharmacological ascorbate as an adjuvant for enhancing radiation-chemotherapy responses in gastric adenocarcinoma. Radiat Res 2018;189:456–465. [PubMed: 29547353]
30. Menon SG, Sarsour EH, Spitz DR, et al. Redox regulation of the G1 to S phase transition in the mouse embryo fibroblast cell cycle. Cancer Res 2003;63:2109–2117. [PubMed: 12727827]
31. Ahmad IM, Aykin-Burns N, Sim JE, et al. Mitochondrial O2*- and H2O2 mediate glucose deprivation-induced stress in human cancer cells. J Biol Chem 2005;280:4254–4263. [PubMed: 15561720]
32. Hauer-Jensen M, Denham JW, Andreyev HJ. Radiation enteropathy—pathogenesis, treatment and prevention. Nat Rev Gastroenterol Hepatol 2014;11:470–479. [PubMed: 24686268]
33. Haydont V, Vozenin-Brotons MC. Maintenance of radiation-induced intestinal fibrosis: Cellular and molecular features. World J Gastroenterol 2007;13:2675–2683. [PubMed: 17569135]
34. Xu B, Kim ST, Lim DS, Kastan MB. Two molecularly distinct G(2)/M checkpoints are induced by ionizing irradiation. Mol Cell Biol 2002;22:1049–1059. [PubMed: 11809797]
35. Patterson JC, Joughin BA, van de Kooij B, Lim DC, Lauffenburger DA, Yaffe MB. ROS and oxidative stress are elevated in mitosis during asynchronous cell cycle progression and are exacerbated by mitotic arrest. Cell Syst 2019;8 163–167.e2. [PubMed: 30797774]
36. Falck J, Petrini JH, Williams BR, Lukas J, Bartek J. The DNA damage-dependent intra-S phase checkpoint is regulated by parallel pathways. Nat Genet 2002;30:290–294. [PubMed: 11850621]
37. Maas M, Beets-Tan RG, Lambregts DM, et al. Wait-and-see policy for clinical complete responders after chemoradiation for rectal cancer. J Clin Oncol 2011;29:4633–4640. [PubMed: 22067400]
38. Habr-Gama A, Gama-Rodrigues J, Sao Juliao GP, et al. Local recurrence after complete clinical response and watch and wait in rectal cancer after neoadjuvant chemoradiation: Impact of salvage therapy on local disease control. Int J Radiat Oncol Biol Phys 2014;88:822–828. [PubMed: 24495589]
39. Vozenin-Brotons MC, Milliat F, Sabourin JC, et al. Fibrogenic signals in patients with radiation enteritis are associated with increased connective tissue growth factor expression. Int J Radiat Oncol Biol Phys 2003;56:561–572. [PubMed: 12738334]
40. Martin M, Lefaix J, Delanian S. TGF-betal and radiation fibrosis: A master switch and a specific therapeutic target? Int J Radiat Oncol Biol Phys 2000;47:277–290. [PubMed: 10802350]
41. Jobling MF, Mott JD, Finnegan MT, et al. Isoform-specific activation of latent transforming growth factor beta (LTGF-beta) by reactive oxygen species. Radiat Res 2006;166:839–848. [PubMed: 17149983]
42. Kim SJ, Denhez F, Kim KY, Holt JT, Sporn MB, Roberts AB. Activation of the second promoter of the transforming growth factor-beta 1 gene by transforming growth factor-beta 1 and phorbol ester occurs through the same target sequences. J Biol Chem 1989;264:19373–19378. [PubMed: 2808430]
43. Bonniaud P, Margetts PJ, Ask K, Flanders K, Gauldie J, Kolb M. TGF-beta and Smad3 signaling link inflammation to chronic fibrogenesis. J Immunol 2005;175:5390–5395. [PubMed: 16210645]
44. Herrera B, Murillo MM, Alvarez-Barrientos A, Beltran J, Fernandez M, Fabregat I. Source of early reactive oxygen species in the apoptosis induced by transforming growth factor-beta in fetal rat hepatocytes. Free Radic Biol Med 2004;36:16–26. [PubMed: 14732287]
45. Hecker L, Vittal R, Jones T, et al. NADPH oxidase-4 mediates myofibroblast activation and fibrogenic responses to lung injury. Nat Med 2009;15:1077–1081. [PubMed: 19701206]

46. Anderson CM, Lee CM, Saunders DP, et al. Phase IIb, randomized, double-blind trial of GC4419 versus placebo to reduce severe oral mucositis due to concurrent radiotherapy and cisplatin for head and neck cancer. J Clin Oncol 2019;37:3256–3265. [PubMed: 31618127]

47. El-Mahdy MA, Alzarie YA, Hemann C, Badary OA, Nofal S, Zweier JL. The novel SOD mimetic GC4419 increases cancer cell killing with sensitization to ionizing radiation while protecting normal cells. Free Radic Biol Med 2020;160:630–642. [PubMed: 32739595]

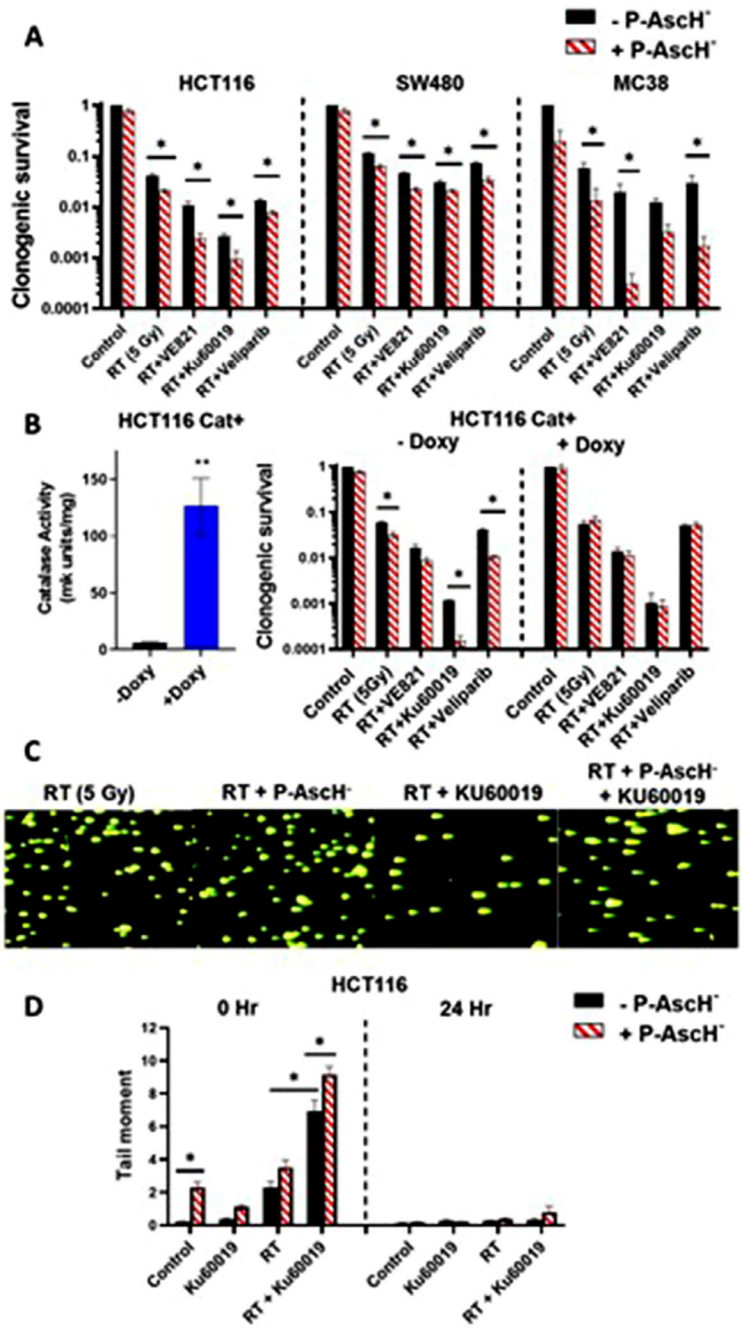

Fig. 1.

Pharmacologic ascorbate ($P\text{-}AscH^{-}$) enhances radiosensitization and DNA damage with ataxia telangiectasia mutated kinase (ATM) inhibitors in colorectal cancer (CRC) models by enhancing H_2O_2 fluxes. (A) CRC cells were treated with radiation therapy (RT) (5 Gy) ± VE821, KU60019, or veliparib ± $P\text{-}AscH^{-}$ (5 pmol/cell) and clonogenic survival was assessed. (B) Clonogenic survival assays were repeated in HCT116cat+ tumors ± doxycycline (doxy) pretreatment. (C,D) Quantification of DNA strand breaks in HCT116 tumor cells after RT (5 Gy), $P\text{-}AscH^{-}$ (5 pM/cell), and KU60019 (1 μM) was performed using neutral COMET assays. Representative images for each RT treatment condition at 0

hour are shown (C) along with graphical comparisons at 0 and 24 hours (D). Bars represent mean ± SEM. n = 3-5 per treatment condition. *$P < .05$ between indicated groups. **$P < .05$ compared with all other groups. *Abbreviations*: HCT = human colon tumor; SEM = standard error of the mean.

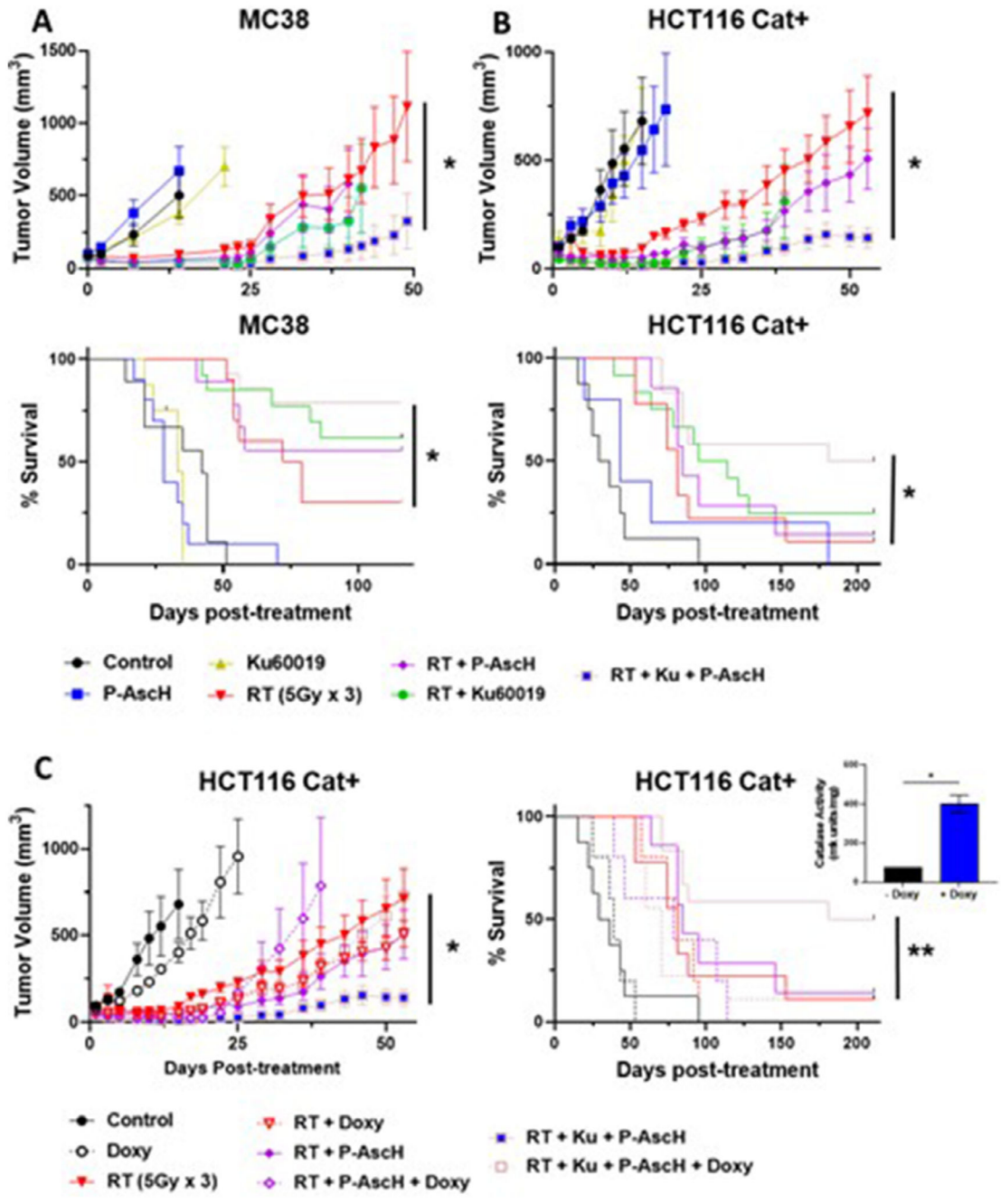

Fig. 2.

Pharmacologic ascorbate ($P\text{-}AscH^{-}$) improves tumor growth delay and survival in combination with radiation therapy (RT) and ataxia telangiectasia mutated kinase (ATM) inhibition. (A) In vivo tumor growth delay curves and survival estimates for mice with MC38 (A) and HCT116cat+ (B) tumors treated with RT (5 Gy × 3) ± KU60019 ± $P\text{-}AscH^{-}$. (C) Tumoral catalase expression was induced by adding doxycycline to the drinking water (quantification is shown in the inset). Fig E2 shows individual growth curves. n = 5-10 for non-RT treatment groups and 8 to 14 for RT treatment groups. *$P < .05$ between indicated groups. **$P < .05$ compared with RT only. *Abbreviation*: HCT = human colon tumor.

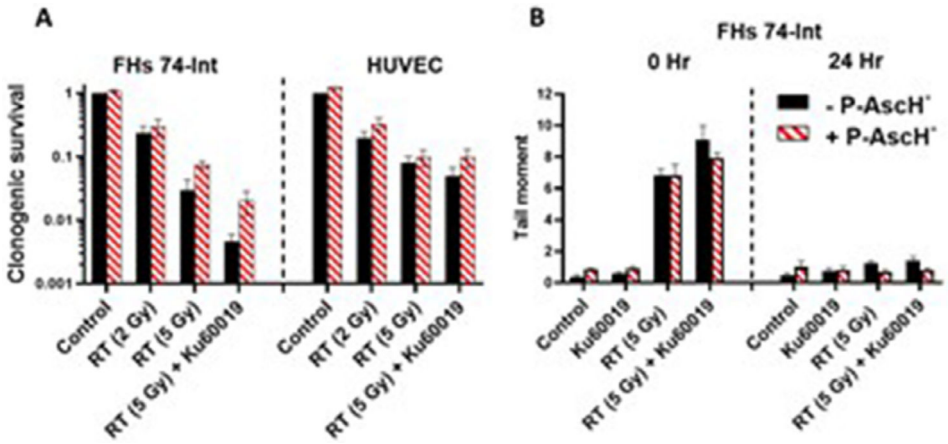

Fig. 3.

Pharmacologic ascorbate (P-AscH$^-$) does not enhance radiosensitization or DNA damage in cultured normal (non-malignant) cells. (A) Clonogenic survival assays in nonmalignant FHs74 and HUVEC cells after treatment with radiation therapy (RT) ± P-AscH = ± KU60019. (B) Neutral COMET assays 0 and 24 hours after treatment in FHs74 cells. Bars represent mean ± SEM. n = 3-5 per treatment condition. *Abbreviations*: HUVEC = human umbilical vein endothelial cells; SEM = standard error of the mean.

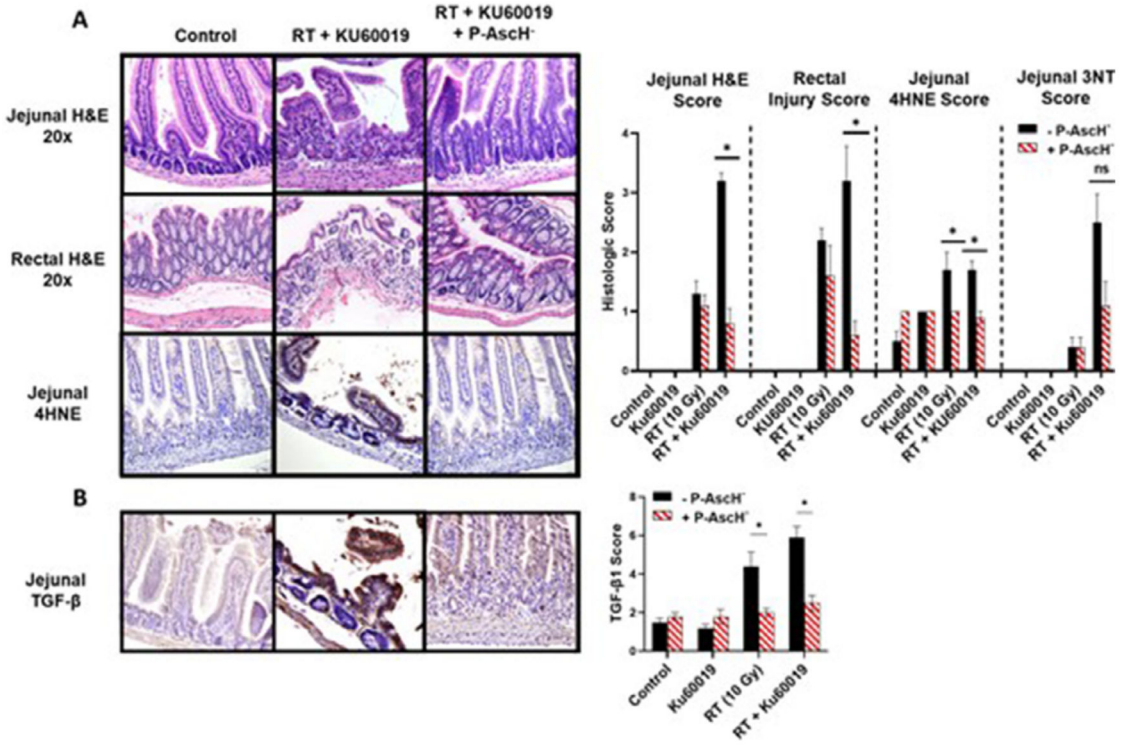

Fig. 4.

Pharmacologic ascorbate (P-AscH$^-$) reduces small and large bowel injury, oxidative damage, and transforming growth factor (TGF)-β immunoreactivity after radiation therapy (RT) and KU60019. (A) Representative photos of jejunal H&E, rectal H&E, and jejunal 4-hydroxynoneal (4HNE) samples 72 hours after treatment with quantitative comparisons. (B) Representative photos of jejunal TGF-β immunofluorescence 72 hours post-RT with quantitative comparisons. Bars shown mean =h SEM. n = 5 for all non-RT conditions and 10 for all RT conditions. *$P < .05$ between indicated groups. 3NT = 3-nitrtyrosine. *Abbreviations*: H&E = hematoxylin and eosin stain; SEM = standard error of the mean.

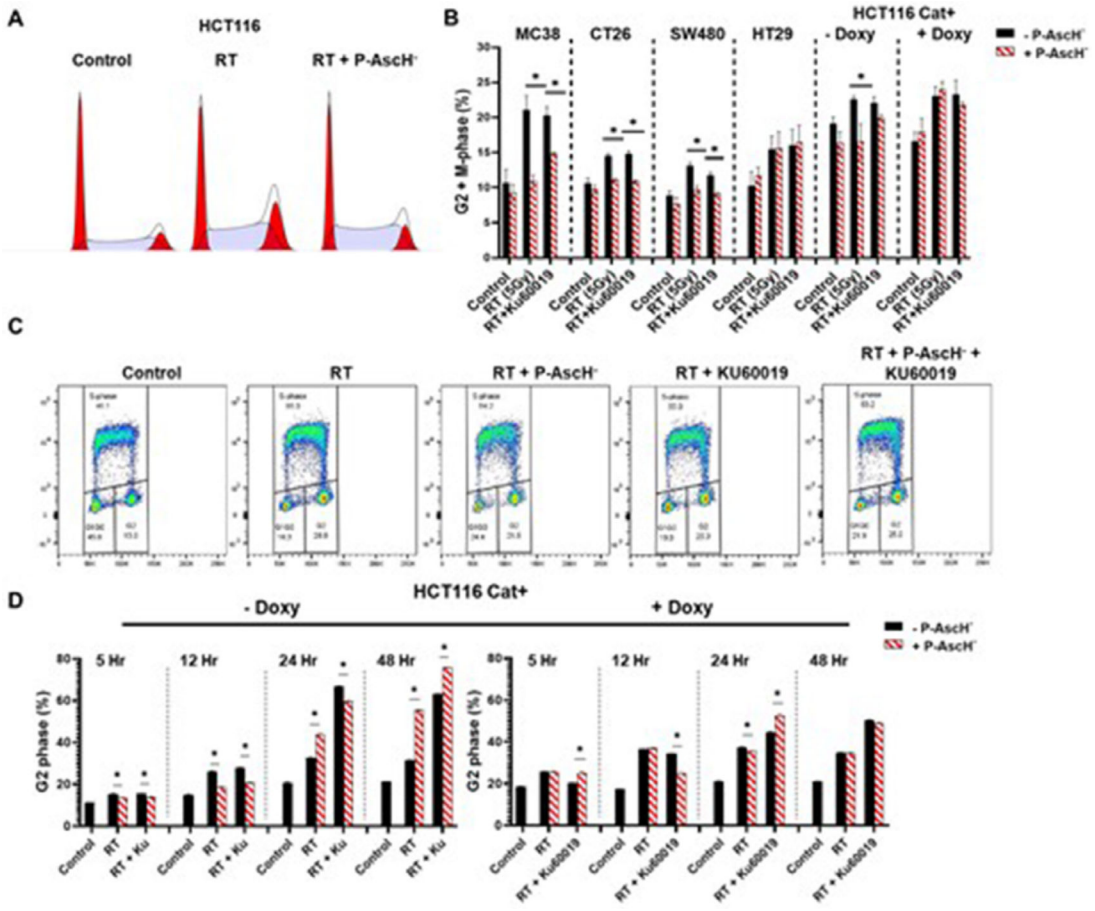

Fig. 5.

Pharmacologic ascorbate (P-AscH$^-$) perturbs G_2+ M-phase cell cycle progression after radiation therapy (RT) ± KU60019. (A) Representative graphs of propidium iodide (PI) cell cycle flow cytometry of the entire cell cycle 5 hours post-RT in HCT116 cells. (B) The proportion of cells in G_2/M 5 hours posttreatment in indicated cell lines is shown for each treatment. (C) Representative images of bromodeoxyuridine (BrdU) + PI flow cytometry dot plots for HCT116 Cat+ cells 12 hours post-RT. (D) Summary data of G_2 phase at 0, 5, 12, 24, and 48 hours post-RT (5 Gy) ± KU60019 ± P-AscH$^-$ in HCT116 Cat+ cells ± doxycycline. Results of all cell cycle phases are shown in Fig E4. Bars shown mean ± SEM. n = 3 for all treatments. *P < .05 between indicated groups. *Abbreviations*: HCT = human colon tumor; SEM = standard error of the mean.

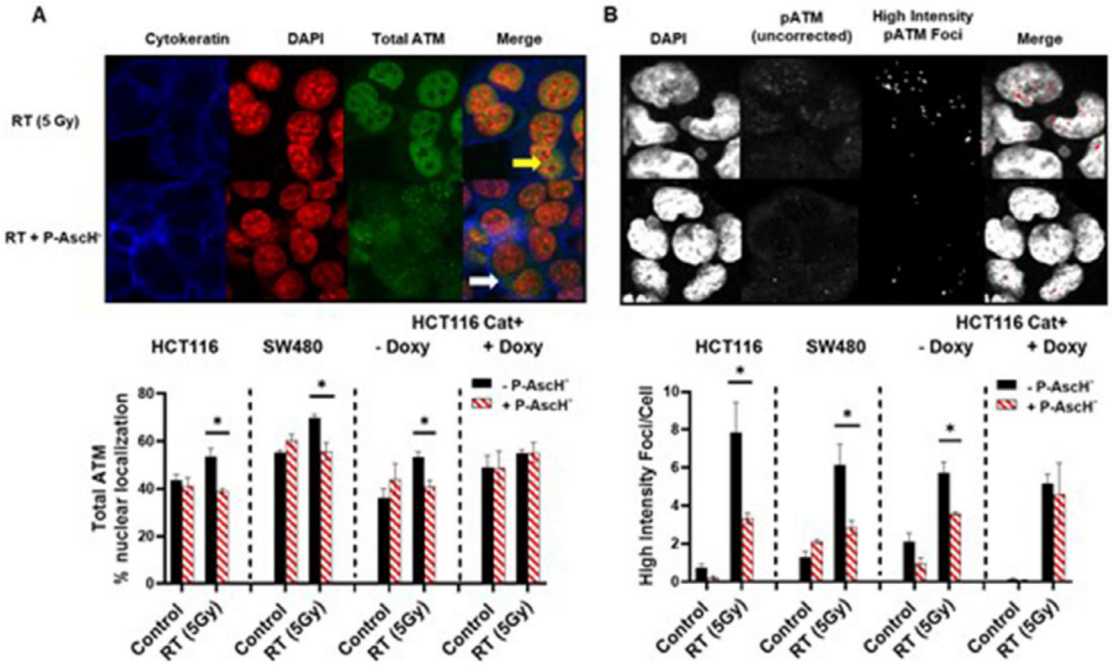

Fig. 6.

Pharmacologic ascorbate ($P\text{-}AscH^{-}$) induces H_2O_2 dependent inhibition of nuclear ataxia telangiectasia mutated kinase (ATM) localization after radiation therapy (RT). (A) Representative images of HCT116 tumor cells stained for cytokeratin (blue), DAPI (red), total ATM (green), and merged images. Nuclear and cytoplasmic localization are indicated by yellow and white arrows, respectively. (B) Representative images showing HCT116 cells 2 hours post-RT for DAPI, uncorrected primary antibody (pATM), high intensity pATM foci (after background subtraction), and overlay of pATM foci (red) and DAPI. Nuclear pATM was quantified 0, 2, and 24 hours post-RT in colorectal cancer (CRC) cells as a function of HIF and integrated density (2 hour timepoints for HIF shown here; remaining data are in Fig. E5). Bars indicate mean ± SEM. n = 3-5 per treatment condition. $*P <$ .05 between indicated groups. *Abbreviations*: DAPI = 4',6'-diamidino-2-phenylindole stain; HCT = human colon tumor; HIF = high intensity foci; SEM = standard error of the mean.